electronics

MDPI

Article

A Pulsed Coding Technique Based on Optical UWB Modulation for High Data Rate Low Power Wireless Implantable Biotelemetry

Andrea De Marcellis [1,*], Elia Palange [1], Luca Nubile [1], Marco Faccio [1], Guido Di Patrizio Stanchieri [1] and Timothy G. Constandinou [2]

[1] Department of Industrial and Information Engineering and Economics, University of L'Aquila, L'Aquila 67100, Italy; elia.palange@univaq.it (E.P.); luca.nubile@graduate.univaq.it (L.N.); marco.faccio@univaq.it (M.F.); guido.dipatriziostanchieri@student.univaq.it (G.D.P.S.)

[2] Centre for Bio-Inspired Technology, Imperial College London, London SW7 2AZ, UK; t.constandinou@imperial.ac.uk

* Correspondence: andrea.demarcellis@univaq.it; Tel.: +39-086-243-4424

Academic Editors: Enzo Pasquale Scilingo and Gaetano Valenza
Received: 14 June 2016; Accepted: 10 October 2016; Published: 17 October 2016

Abstract: This paper reports on a pulsed coding technique based on optical Ultra-wideband (UWB) modulation for wireless implantable biotelemetry systems allowing for high data rate link whilst enabling significant power reduction compared to the state-of-the-art. This optical data coding approach is suitable for emerging biomedical applications like transcutaneous neural wireless communication systems. The overall architecture implementing this optical modulation technique employs sub-nanosecond pulsed laser as the data transmitter and small sensitive area photodiode as the data receiver. Moreover, it includes coding and decoding digital systems, biasing and driving analogue circuits for laser pulse generation and photodiode signal conditioning. The complete system has been implemented on Field-Programmable Gate Array (FPGA) and prototype Printed Circuit Board (PCB) with discrete off-the-shelf components. By inserting a diffuser between the transmitter and the receiver to emulate skin/tissue, the system is capable to achieve a 128 Mbps data rate with a bit error rate less than 10^{-9} and an estimated total power consumption of about 5 mW corresponding to a power efficiency of 35.9 pJ/bit. These results could allow, for example, the transmission of an 800-channel neural recording interface sampled at 16 kHz with 10-bit resolution.

Keywords: high data rate low power link; optical ultra-wideband modulation; pulsed coding technique; wireless implantable biotelemetry

1. Introduction

Emerging implantable biomedical systems need to transmit large amounts of data through skin/tissue to achieve high accuracy measurements, high dimensionality and real-time control of complex prosthetic devices like brain machine interfaces [1–3]. These systems require wireless biotelemetry links with high data rate, reduced power consumption, small Bit Error Rate (BER) and good electromagnetic compliance [3–7]. Solutions that make use of carrier-based narrow-band and Ultra-wideband (UWB) Radio Frequency (RF) links, employing Impulse Radio (IR) signal modulation, pose significant challenges when requiring high data rates due to their low power efficiency and electromagnetic compatibility [8–13]. Optical biotelemetry links, employing semiconductor modulated/pulsed lasers as data transmitters and photodiodes as data receivers, allow the performances of the RF-based systems to be enhanced [4,14–17]. In these regards, further improvements have been obtained by increasing the laser power and by using On-Off Keying (OOK) based modulations and large sensitive area photodiodes. However, this solution increases the laser response

time and BER so limiting system bandwidth and data rate up to 100 Mbps with 21 pJ/bit power efficiency [4,15].

This Paper presents a data coding technique based on optical UWB modulation employing sub-nanosecond laser pulses with duration much smaller than the half bit period as typically employed in OOK modulation-based solutions. In particular, the proposed approach, already investigated in IR-UWB systems [13], implements an optical synchronised-OOK modulation allowing for the clock recovery and a proper synchronisation between the transmitter and the receiver. In general, optical UWB communication systems using modulated/pulsed signals have the advantages of low power spectral density, null RF interference, immunity to multipath fading and high power efficiency, so suitable for short-range wireless links [17–20]. Based also on these characteristics, the proposed approach allows us to strongly reduce the system overall power consumption and the laser response time reaching data rates up to 128 Mbps with 800 ps laser pulses, a bit period of 7.8 ns and a power efficiency of 35.9 pJ/bit. These results have been obtained by adjusting the amplitude and duration of the laser pulses to achieve the optimal trade-off between power consumption, data rate and BER. Respect to the state-of-the-art, the implemented pulsed coding technique is capable to increase the data rate (i.e., the transmission bandwidth) and, at the same time, to strongly reduce the power consumption (i.e., better power efficiency) of the optical communication system that is mainly related to the generation of the sub-nanosecond laser pulses. The presented architecture has been implemented on Field-Programmable Gate Array (FPGA) and prototype Printed Circuit Board (PCB) developed with discrete off-the-shelf components. The achieved results enable, for example, the transmission of an 800-channel neural recording interface (i.e., extracellular electrodes) sampled at 16 kHz with 10-bit resolution [21,22].

2. The Pulsed Coding Technique: Theory, Modelling and Methods of the Optical Approach

Figure 1 illustrates the top-level complete architecture of an optical wireless transcutaneous biotelemetry system. The dashed black square box highlights the scheme implementing the proposed optical pulsed UWB modulation technique performing the data coding process. The overall system typically includes two units, implantable and external, each one consisting of a main sub-block: the transmitter and the receiver.

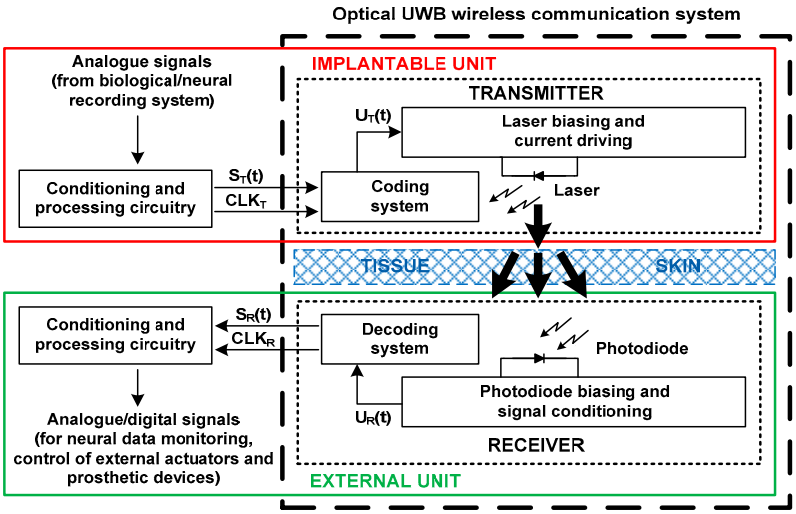

Figure 1. Complete scheme of an optical wireless transcutaneous biotelemetry system: in the dashed box, the architecture implementing the proposed data coding approach based on optical pulsed Ultra-wideband (UWB) modulation technique.

The conditioning and processing circuitry block in the implantable unit handles analogue signals related to neural signals (e.g., coming from neural recording systems) [21,22]. The analogue signals

are converted into a serial digital data stream $S_T(t)$ to be transmitted, after its coding in pulsed signal $U_T(t)$, from the implantable to the external unit. The receiver in the external unit provides the decoded/regenerated serial digital data stream $S_R(t)$ to the related conditioning and processing circuitry block. The latter, in this case, generates analogue and/or digital signals associated to the transmitted neural analogue signals for the control of external actuators as well as for neural data monitoring.

More in detail, the transmitter takes, as input signals, the main clock CLK_T and the data stream $S_T(t)$ to be coded and transferred, while the receiver provides the recovered clock signal CLK_R and the decoded data stream $S_R(t)$. In the transmitter, the coding system generates the analogue pulsed voltage signal $U_T(t)$ converted by the bias and drive circuits into current pulses that generate the laser pulses (i.e., gain switching operation of the laser). In the receiver, the photodiode provides photocurrent pulses converted by the biasing and signal conditioning circuitry into analogue voltage pulses $U_R(t)$ processed by the decoding system that recovers the clock CLK_R and the data stream $S_R(t)$. The transmitter uses a high speed Vertical Cavity Surface Emitting Laser (VCSEL) generating sub-nanosecond optical pulses and the receiver employs a wide bandwidth Si photodiode.

Figure 2 illustrates an example of a timing diagram, with the corresponding laser operating conditions, describing the proposed data coding process that allows the optical pulsed UWB modulation performed by the transmitter to be achieved. During each bit period T, the VCSEL driving current is maintained at a value $I_{\min}$ just above the VCSEL threshold current I_{th} (corresponding to a minimum laser power $P_{\min}$) to provide high output power stability, few picoseconds rise times and negligible jitter respect to the driving current pulses. In order to simultaneously transmit the CLK_T and $S_T(t)$, short current pulses with a maximum value $I_{\max}$ drive the VCSEL that generates optical pulses with a power $P_{\max}$. Therefore, only during the laser pulse generation the transmitter achieves the maximum power consumption. Depending on the receiver performances, the current pulse amplitude and duration can be adjusted to obtain the optimal trade-off between power consumption, data rate and BER. More in detail, referring to Figure 2, at the start of each bit period T a short laser pulse is generated, independently from the symbol being transmitted, so allowing for the clock signal to be simultaneously transmitted with the symbol. This is needed to synchronise the transmitter and the receiver (i.e., the clock recovery procedure). Then, at half bit period $T/2$, if the symbol 1 has to be transmitted, a second laser pulse is generated, while for the transmission of the symbol 0 the VCSEL driving current is maintained at the value $I_{\min}$. In this way, the transmitter power consumption is mainly due to the current $I_{\min}$ that is constant during each bit period T, while the contribution of the current pulses, with an amplitude equal to $I_{\max}$, is minimal due to the very small duty cycle. These operating conditions allow us to strongly reduce the system overall power consumption and the VCSEL response time.

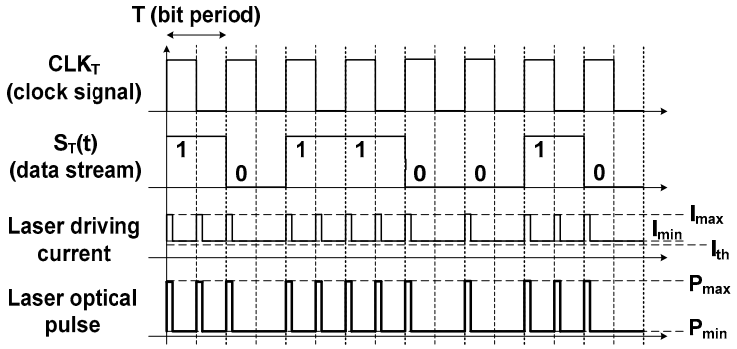

Figure 2. Example of a timing diagram describing the proposed data coding process and the corresponding laser operating conditions.

Figure 3 shows the logic block level implementation of the coding and decoding systems inside the transmitter and the receiver, respectively. The coding system receives in input CLK_T and $S_T(t)$ considering the bit period T equal to the clock period (i.e., one bit transmitted at each bit period T), as shown in Figure 2 and detailed in Figure 4a.

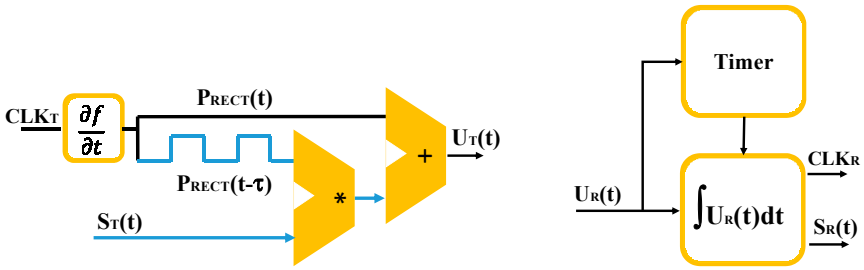

Figure 3. Description, at logic block level, of the implementation of the coding (on the **left**); and decoding (on the **right**) systems.

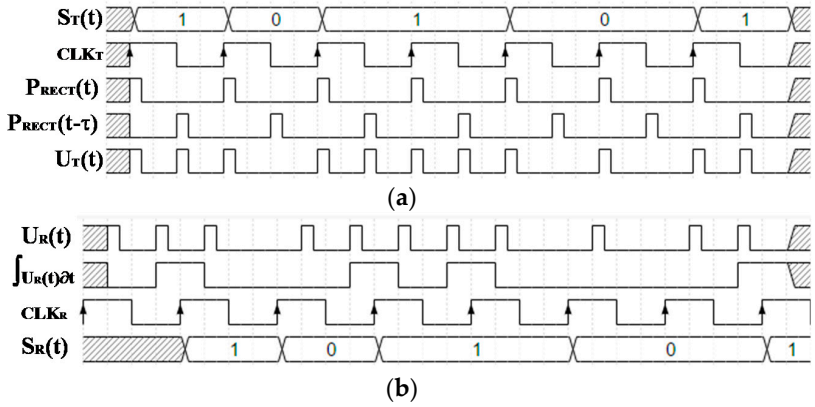

Figure 4. Correlations between the signals $\mathrm{CLK}_{T,R}$, $S_{T,R}(t)$ and the corresponding coded data $U_{T,R}(t)$ related to the coding (**a**); and decoding (**b**) systems.

Thus, the coding system generates a train of "rect" pulses $P_{\mathrm{RECT}}(t) = \sum_{n=-\infty}^{+\infty} \left[\mathrm{rect}_{T_0}(t - nT)\right]$ having a period T with a very small duty cycle T_0 and the same signal, delayed by a time period $\tau = T/2$, defined as $P_{\mathrm{RECT}}(t-\tau) = \sum_{n=-\infty}^{+\infty} \left[\mathrm{rect}_{T_0}(t - nT - \tau)\right]$. The transmitted pulsed signal $U_T(t)$ is obtained as the combination of $P_{\mathrm{RECT}}(t)$ and $P_{\mathrm{RECT}}(t-\tau)$ and can be expressed as follows:

$$U_T(t) = \sum_{n=-\infty}^{+\infty} \left[\mathrm{rect}_{T_0}(t - nT) + S_T(t) * \mathrm{rect}_{T_0}(t - nT - \tau)\right] \quad (1)$$

On the other hand, $U_T(t)$ contains the constant pulses $P_{\mathrm{RECT}}(t)$ used for the clock recovery and the pulses $P_{\mathrm{RECT}}(t-\tau)$ related to the transmitted data $S_T(t)$ (i.e., the bit symbols 1 or 0). Inversely, $U_R(t)$ is the input of the decoding system that operates clock and data recovery so providing the synchronisation signal CLK_R and the decoded data stream $S_R(t)$. In particular, the decoding system integrates the signal $U_R(t)$ during a bit period T, starting from $T/2$ after the first synchronisation pulse through the "Timer" block (see Figure 3), according to the following relation:

$$S_R(t) = \begin{cases} 1 \text{ if } \int_{T/2}^{T} U_R(t)\,dt \geq t_H \\ \\ 0 \text{ if } \int_{T/2}^{T} U_R(t)\,dt \leq t_L \end{cases} ; \text{ Err } \forall \quad (2)$$

where t_H and t_L are the high and low threshold levels defined by the decoding system. Consequently, the generated output signals $S_R(t)$ and CLK_R can be described as detailed in Figure 4b. More in detail,

since the clock recovery as well as the synchronisation between the transmitter and the receiver is a critical issue in communication systems, the "Timer" block includes a control unit. Starting from the pulsed signal $U_R(t)$, the control unit operates the clock recovery by managing the regeneration of the new clock signal CLK_R and its synchronisation with the received pulses $U_R(t)$. Simultaneously, the overall "Timer" block also controls the synchronisation between the recovered clock CLK_R and the integrator block that, in turn, performs the recovery and regeneration of the data stream $S_R(t)$. In particular, the control unit accomplishes these operations by regulating the relative time delays (i.e., the timing alignments) between the received pulse train $U_R(t)$ and the recovered clock CLK_R together with the integration window, from $T/2$ to T, of the integrator block to correctly recover the data stream $S_R(t)$.

3. Implementation of the Wireless Communication System Based on the Pulsed Coding Technique

The optical pulsed UWB wireless communication system, performing the proposed data coding process, has been characterised by implementing the coding and decoding digital systems (see Figure 3) on an FPGA board (Xilinx VIRTEX-6 ML605, Xilinx Inc., San Jose, CA, USA) by a hardware description (VHDL, that is VHSIC Hardware Description Language where VHSIC means Very High Speed Integrated Circuits) of the functional/logic blocks previously described. The FPGA was used to: (i) supply the CLK_T and $S_T(t)$ signals at the input of the coding system that generates $U_T(t)$; (ii) recover the CLK_R and $S_R(t)$ from the received $U_R(t)$ through the decoding system. The resulting digital architecture is composed by a 2:1 multiplexer, a 1:2 demultiplexer, three D-type flip-flops and 22 logic gates (AND, OR, NOT). The corresponding circuitry can be implemented in standard Complementary Metal-Oxide Semiconductor (CMOS) technology as a full-custom solution with less than 150 transistors in a Si area smaller than 1 mm^2.

The employed laser is a high-speed VCSEL-850 (Thorlabs Inc., Newton, NJ, USA) with 2.2 mA threshold current emitting at λ = 845 nm. This wavelength has been chosen considering the best light "penetration window" of human skin that ranges between 800 nm and 1300 nm [23].

The photodiode is the Si high-speed FDS025 (Thorlabs Inc., Newton, NJ, USA) with 47 ps rise time and 49,000 μm^2 sensitive area. All analogue circuits have been implemented on prototype PCB using high-bandwidth discrete off-the-shelf components. In particular, the VCSEL biasing and driving current circuitry has been implemented by employing the driver ADN2871 (Analog Devices Inc., Norwood, MA, USA) operating a voltage-to-current conversion. The output DC bias current was set to 2.25 mA (i.e., I_{min}, see Figure 2) just about 2.5% above the VCSEL threshold current I_{th}, while the peak value of the current pulses was regulated up to a maximum value of 4.5 mA (i.e., $I_{max} = 2I_{min}$). The photodiode biasing and signal conditioning circuitry has been implemented by using the ultra-low noise voltage-feedback operational amplifier OPA847 (Texas Instruments Inc., Dallas, TX, USA) configured as a transimpedance amplifier to convert the generated pulsed photocurrent into voltage pulses (i.e., a current-to-voltage conversion). This stage is combined with ADN2915 (Analog Devices Inc., Norwood, MA, USA) that includes a limiting amplifier and a signal level detector.

4. Experimental Results and Discussion

Experimental measurements were performed with the implemented overall system operating at different data rates up to 128 Mbps employing a Pseudo-Random Bit Sequence (PRBS) of length 2^{31}-1 (i.e., the data stream) generated by the FPGA board with an average number of pulses transmitted for each bit equal to 1.5 pulses/bit. Moreover, a 1.5 mm thick diffuser ED1-C20-MD (Thorlabs Inc., Newton, NJ, USA) was inserted between the VCSEL and the photodiode to emulate the presence of skin or tissue [11,23]. For the considered distances between the VCSEL and the photodiode of only few millimetres, the diffuser reduces the laser power of about a factor 10. Furthermore, the transmission channel could be considered as a "noisy channel" and the BER has been directly evaluated through experimental measurements since it depends on the channel condition mainly related to the employed

diffuser. More in detail, the BER has been evaluated through the FPGA board considering the system under different working conditions: variations of the laser pulse amplitude and duration as well as changes of the distance between the VCSEL and the photodiode. In particular, in the operating conditions at 128 Mbps, the bit period T is 7.8 ns and the laser pulse duration was reduced to about 800 ps corresponding to a duty-cycle T_0 of 10%. This system set-up allowed us to achieve the optimum trade-off between data rate, BER and power consumption. In principle, for a fixed data rate, the duty-cycle T_0 of the pulses (i.e., the laser pulse duration) can be reduced providing lower power consumptions at the expenses of an increase of the BER value. On the contrary, for achieving a minimum fixed BER value, it is possible to decrease the duty-cycle of the laser pulses providing a lower power consumption against a reduction of the data rate that, in some case, could imply a worst system power efficiency. In our case, at 128 Mbps transmission data rate and T_0 = 10% laser pulse duty-cycle, the highest measured BER is less than 10^{-9}, achieved for a total maximum distance lower than 4 mm including the presence of the diffuser, with an estimated maximum total power consumption of the overall system of about 5 mW, the 10% of which is related to the coding and decoding digital systems. In this regard, any clock synchronisation mismatch affecting a correct data communication has been also taken into account in the evaluation of the BER since timing misalignments of the clock signal (i.e., clock synchronisation errors) provide bit errors in the decoding system. In addition, it is important to consider that in the proposed architecture, the coding system in the transmitter block does not include any error-correction process that further would improve the BER. In this sense, for example, Hamming and Golay error-correction codes could be considered as suitable solutions to be implemented by an additional low power circuitry enhancing the BER of few orders of magnitude with an additional energy consumption of only 3–4 pJ/bit [19,20].

Figure 5 reports a picture of the overall implemented system together with the related block scheme of the experimental set-up showing its main components. In particular, the transmitter and the receiver blocks are connected to the FPGA board and the two XYZ translation stages allow us both to perform the optical alignment between the VCSEL and the photodiode and change their relative distance. Figure 6 shows an example of the main signals related to the transmitter and the receiver blocks operating at 128 Mbps. From top to bottom: the green trace is CLK_T, the yellow $S_T(t)$, the purple $U_T(t)$ and the blue $S_R(t)$. In the insets are reported: (A) multiple acquisitions of $U_T(t)$ for the evaluation of the amplitude and phase jitters resulting lower than 150 mV and 100 ps, respectively; (B) the $U_R(t)$ and the related $S_R(t)$ signals; (C) the $S_R(t)$ eye diagram showing amplitude and phase jitters lower than 100 mV and 150 ps, respectively. All the measurements have been performed by using WAVEMASTER 8600A digital oscilloscope (LeCroy). Figure 6 demonstrates that the received and decoded data stream $S_R(t)$ correctly matches with the transmitted one ($S_T(t)$) showing a time delay of about 18 ns mainly due to clock recovery and data decoding processes. Moreover, referring to the inset B) of Figure 6, it has been experimentally evaluated also the overall impulse response of the transmission channel by means of the time-domain analysis of the received pulsed signal $U_R(t)$.

Furthermore, it is important to highlight that the proposed system is not based on IR-UWB modulation and does not employs RF electrical pulses and/or antennas to transmit the modulated/pulsed signals. On the other hand, the duration of the generated optical pulses is lower than 1 ns. Thus, in principle, the proposed architecture implementing the optical pulsed coding technique complies with the standards UWB specifications on the generation of pulsed signals. In this regards, Figure 7 reports the overall power spectrum of the transmitted pulsed signal $U_T(t)$ generated by the coding system showing high spikes that, in principle, could affect the overall power efficiency of the system. Nevertheless, an effective trade-off between transmission data rate, power efficiency and BER has been achieved. In particular, the experimental data demonstrate that the pulse characteristics and specifications comply and satisfy the standard mask defined by the Federal Communications Commission (FCC) on the power spectrum of modulated/pulsed signals (i.e., the power emission limits of the signals for communications) [24]. Moreover, Figure 7 shows a primary lobe with a

bandwidth of about 1.25 GHz corresponding to the inverse of the laser pulse duration (i.e., 1/800 ps) so validating and confirming the theoretical expectations.

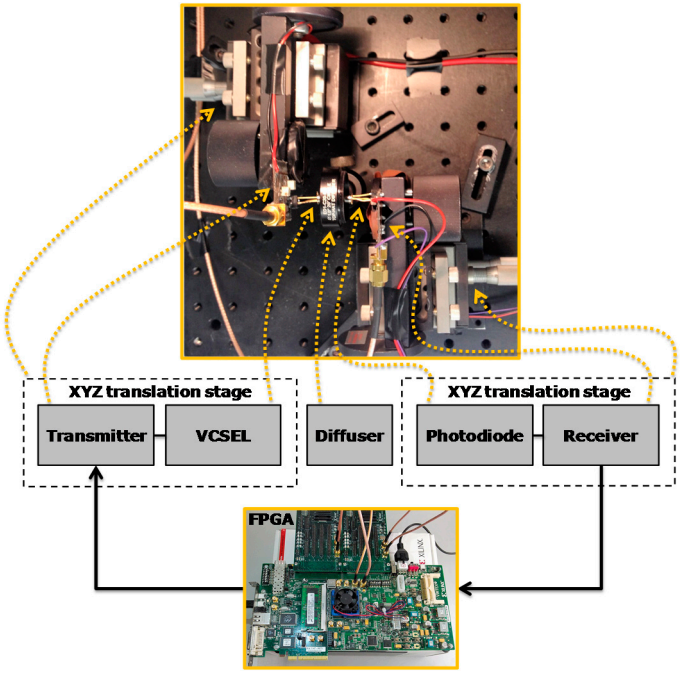

Figure 5. Experimental set-up: picture of the overall implemented system and the related block scheme showing its main components.

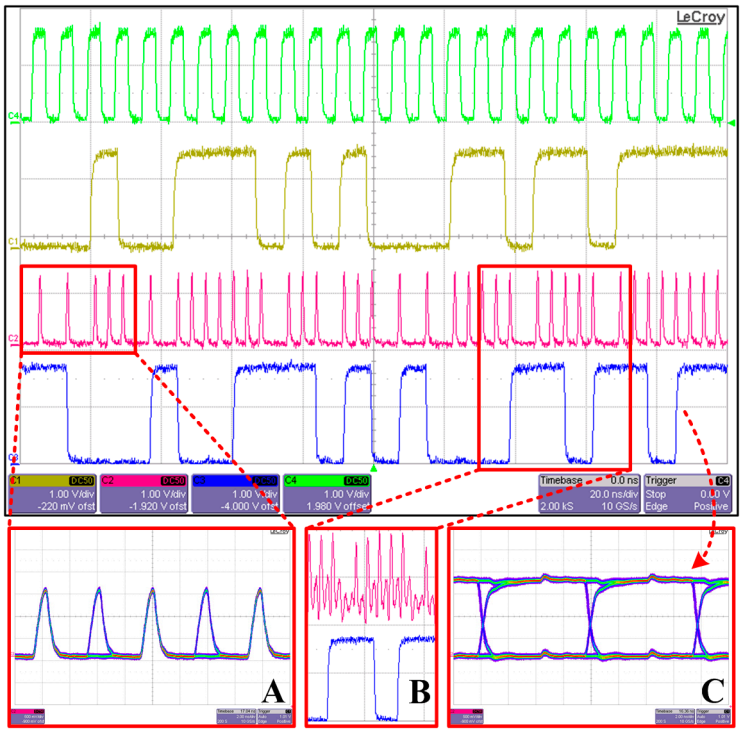

Figure 6. Main signals related to the transmitter and the receiver blocks. From top to bottom: CLK_T (green), $S_T(t)$ (yellow), $U_T(t)$ (purple), $S_R(t)$ (blue). In the insets: (**A**) multiple acquisitions of $U_T(t)$ for the evaluation of the amplitude and phase jitters; (**B**) $U_R(t)$ and the related $S_R(t)$; (**C**) the eye diagram of $S_R(t)$.

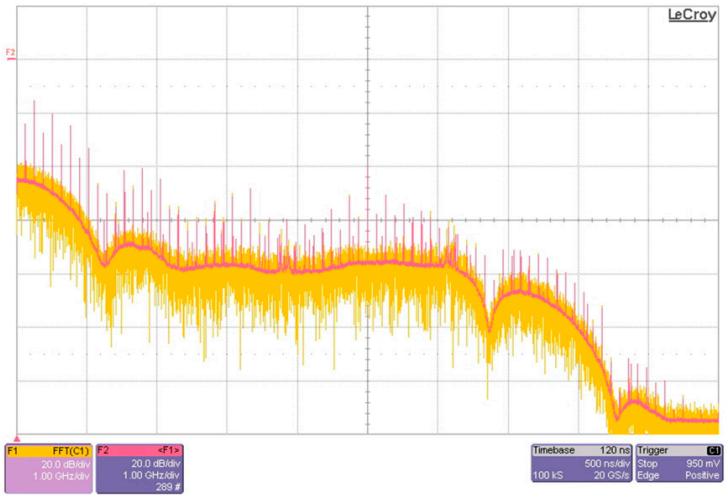

Figure 7. Power spectrum of the transmitted pulsed signal $U_T(t)$ (orange trace) and its average value (purple trace).

Finally, in order to perform a comparative analysis with the state-of-the-art on transcutaneous biotelemetry, Table 1 summarises the main performances of different solutions reported in literature and those ones presented in this Paper. More in detail, in RF-based solutions, high data rates are achieved at low power consumptions and good power efficiencies with high BER values [9,10,12]. A very low BER with a satisfactory data rate are obtained in [11,13] even if at the expenses of a strong increase of the RF system power consumption and power efficiency. Considering now the solutions based on optical wireless links, 100 Mbps is the highest achieved data rate with reduced power consumptions and good power efficiencies and BER values [4,14,15]. This represents the best trade-off among the main parameters of interest. On the other hand, the solution proposed in this paper shows the highest data rate and the best BER value among the optical link solutions. The mean value of the transmitter power consumption is 4.6 mW corresponding to a 35.9 pJ/bit power efficiency of the overall implantable unit. It is worth noting that these values have been obtained by implementing the complete architecture on prototype PCB with discrete off-the-shelf commercial components and using a VCSEL with a relatively high threshold current. Nevertheless, the proposed optical pulsed UWB modulation technique implemented on-chip in a standard CMOS Si technology using VCSEL with lower threshold currents (e.g., Philips-ULM Photonics VCSEL-ULM850-10-TTN0101U with I_{th} = 0.5 mA [15]) could allow the reduction of the transmitter power consumption down to about 1 mW corresponding to a power efficiency of 7.8 pJ/bit. In this case, the estimated maximum total power consumption of the overall system is about 1.5 mW.

Table 1. Main performances of different biotelemetry links.

Reference (Year)	Data Rate (Mbps)	Transmitter Power (mW)	Power Efficiency (pJ/bit)	BER (Bit Error Rate)
[9] (2015)	67	2	30	$<10^{-7}$
[10] (2010)	136	3	22	$<10^{-3}$
[11] (2004)	80	45	562.5	$<10^{-14}$
[12] (2013)	135	1.4	10	-
[13] (2011)	10	1.84	97.5	-
[14] (2007)	40	4.3	107.5	$<10^{-5}$
[15] (2014)	100	2.1	21	$<10^{-7}$
[4] (2015)	100	3.2	32	-
This work	128	4.6 (measured with a VCSEL having I_{th} = 2.2 mA)	35.9	$<10^{-9}$
		1 (estimated with a VCSEL having I_{th} = 0.5 mA)	7.8	

5. Conclusions

The Paper reported on a data coding technique for high data rate low power optical wireless biotelemetry using sub-nanosecond pulsed laser as data transmitter and small sensitive area photodiode as data receiver. The implementation of this approach, based on an optical pulsed UWB synchronised-OOK modulation, through FPGA board and prototype PCB with discrete off-the-shelf components allowed us to achieve a 128 Mbps data rate, a BER less than 10^{-9} and a power efficiency of 35.9 pJ/bit. These values have been obtained by inserting a diffuser between the transmitter and the receiver to emulate skin/tissue barrier. The achieved results demonstrate that the proposed approach enables, for example, the transmission of an 800-channel neural recording interface sampled at 16 kHz with 10-bit resolution for high performances (i.e., high data rate and good power efficiency) optical wireless implantable biotelemetry. The overall architecture that implements the developed technique has been designed to be integrated on-chip in a compact Si footprint lower than 1 mm^2 with about 180 transistors. In this regard, a suitable design of the complete circuitry in a proper standard technology (e.g., Bi-CMOS) and the use of fast pulsed lasers and high-speed photodiodes, will allow us to achieve high performances wireless optical links with data rates up to few Gbps. Finally, the presented optical pulsed coding technique can be also applied to bidirectional transcutaneous biomedical platforms for very high data rate and ultra low power optical wireless biotelemetry that would integrate a transmitter-receiver in the implantable unit and the corresponding receiver-transmitter in the external unit.

Author Contributions: The Authors contributed equally to this work. In particular: Andrea De Marcellis developed the new technique, implemented the analogue circuitry and performed experimental measurements. He contributed to writing and editing the manuscript. He coordinated the manuscript elaboration. Elia Palange optimised the use of the optoelectronic/photonic components, implemented the experimental set-up and analysed the data. He contributed to writing and editing the manuscript. Luca Nubile developed, simulated and implemented the digital architectures on FPGA. He contributed to writing and editing the manuscript. Marco Faccio developed the digital architectures and analysed the data. He contributed to writing and editing the manuscript. Guido Di Patrizio Stanchieri simulated and implemented the digital architectures on FPGA and performed tests and experimental measurements. He contributed to writing and editing the manuscript. Timothy G. Constandinou supplied the overall system specifications and constrains, contributed in theoretical discussions and analysed the data. He contributed to writing and editing the manuscript.

Conflicts of Interest: The authors declare no conflict of interest.

References

1. Park, J.H.; Jeong, J.; Moon, H.; Kim, C.; Kim, S.J. Feasibility of LCP as an encapsulating material for photodiode-based retinal implants. *IEEE Photonics Technol. Lett.* **2016**, *28*, 1018–1021. [CrossRef]
2. Keith-Hynes, P.; Mize, B.; Robert, A.; Place, J. The diabetes assistant: A smartphone-based system for real-time control of blood glucose. *Electronics* **2014**, *3*, 609–623. [CrossRef]
3. Yuan, H.; He, B. Brain–computer interfaces using sensorimotor rhythms: Current state and future perspectives. *IEEE Trans. Biomed. Eng.* **2014**, *61*, 1425–1435. [CrossRef] [PubMed]
4. Liu, T.; Anders, J.; Ortmanns, M. Bidirectional optical transcutaneous telemetric link for brain machine interface. *IET Electron. Lett.* **2015**, *51*, 1969–1971. [CrossRef]
5. Duncan, K.; Etienne-Cummings, R. Selecting a safe power level for an indoor implanted UWB wireless biotelemetry link. In Proceedings of the 2013 IEEE Biomedical Circuits and Systems Conference, Rotterdam, The Netherlands, 31 October–2 November 2013; pp. 230–233.
6. Rush, A.D.; Troyk, P.R. A power and data link for a wireless-implanted neural recording system. *IEEE Trans. Biomed. Eng.* **2012**, *59*, 3255–3262. [CrossRef] [PubMed]
7. Vračar, L.; Prijić, A.; Nešić, D.; Dević, S.; Prijić, Z. Photovoltaic energy harvesting wireless sensor node for telemetry applications optimized for low illumination levels. *Electronics* **2016**, *5*. [CrossRef]
8. Miranda, H.; Gilja, V.; Chestek, C.A.; Shenoy, K.V.; Meng, T.H. A high-rate long-range wireless transmission system for simultaneous multichannel neural recording applications. *IEEE Trans. Biomed. Circuits Syst.* **2010**, *4*, 181–191. [CrossRef] [PubMed]

9. Ebrazeh, A.; Mohseni, P. 30 pJ/b, 67 Mbps, centimeter-to-meter range data telemetry with an IR-UWB wireless link. *IEEE Trans. Biomed. Circuits Syst.* **2015**, *9*, 362–369. [CrossRef] [PubMed]
10. Jung, J.; Zhu, S.; Liu, P.; Emery-Chen, Y.J.; Heo, D. 22-pj/bit energy-efficient 2.4-GHz implantable OOK transmitter for wireless biotelemetry systems: In vitro experiments using rat skin-mimic. *IEEE Trans. Microw. Theory Tech.* **2010**, *58*, 4102–4111. [CrossRef]
11. Guillory, K.S.; Misener, A.K.; Pungor, A. Hybrid RF/IR transcutaneous telemetry for power and high-bandwidth data. In Proceedings of the 2004 IEEE Engineering in Medicine and Biology Societ, San Francisco, CA, USA, 1–5 September 2004; pp. 4338–4340.
12. Elzeftawi, M.; Theogarajan, L. A 10 pJ/bit 135 Mbps IR-UWB transmitter using Pulse Position Modulation and with on-chip LDO regulator in 0.13 μm CMOS for biomedical implants. In Proceedings of the 2013 IEEE Topical Conference on Biomedical Wireless Technologies, Networks, and Sensing Systems, Austin, TX, USA, 20–23 January 2013; pp. 37–39.
13. Crepaldi, M.; Li, C.; Fernandes, J.; Kinget, P. An ultra-wideband impulse-radio transceiver chipset using synchronized-OOK modulation. *IEEE J. Solid-State Circuits* **2011**, *46*, 2284–2299. [CrossRef]
14. Ackermann, D. High Speed Transcutaneous Optical Telemetry Link. Master's Thesis, Case Western Reserve University, Cleveland, OH, USA, May 2007.
15. Liu, T.; Bihr, U.; Becker, J.; Anders, J.; Ortmanns, M. In vivo verification of a 100 Mbps transcutaneous optical telemetric link. In Proceedings of the 2014 IEEE Biomedical Circuits and Systems Conference, Lausanne, Switzerland, 22–24 October 2014; pp. 580–583.
16. Kuchta, D.M.; Rylyakov, A.V.; Doany, F.E.; Schow, C.L.; Proesel, J.E.; Baks, C.W.; Westbergh, P.; Gustavsson, J.S.; Larsson, A. A 71-Gb/s NRZ modulated 850-nm VCSEL-based optical link. *IEEE Photonics Technol. Lett.* **2015**, *27*, 577–580. [CrossRef]
17. Wen, Y.H.; Feng, K.M. A simple NRZ-OOK to PDM RZ-QPSK optical modulation format conversion by bidirectional XPM. *IEEE Photonics Technol. Lett.* **2015**, *27*, 935–938. [CrossRef]
18. Chenhui, Y.; Kun, Z.; Hongyan, F.; Sailing, H. An all-optical transformer from differential NRZ data to Ultra-Wideband pulse stream. *IEEE Photonics Technol. Lett.* **2011**, *23*, 579–581.
19. Desset, C.; Fort, A. Selection of channel coding for low-power wireless systems. In Proceedings of the 2003 IEEE Vehicular Technology Conference, Orlando, FL, USA, 22–25 April 2003; pp. 1920–1924.
20. Hannan, M.A.; Abbas, S.M.; Samad, S.A.; Hussain, A. Modulation Techniques for Biomedical Implanted Devices and Their Challenges. *Sensors* **2012**, *12*, 297–319. [CrossRef] [PubMed]
21. Barsakcioglu, Y.D.; Liu, Y.; Bhunjun, P.; Navajas, J.; Eftekhar, A.; Jackson, A.; Quiroga, R.Q.; Constandinou, T.G. An analogue front-end model for developing neural spike sorting systems. *IEEE Trans. Biomed. Circuits Syst.* **2014**, *8*, 216–227. [CrossRef] [PubMed]
22. Montoye, A.H.; Dong, B.; Biswas, S.; Pfeiffer, K.A. Use of a Wireless Network of Accelerometers for Improved Measurement of Human Energy Expenditure. *Electronics* **2014**, *3*, 205–220. [CrossRef] [PubMed]
23. Bashkatov, A.N.; Genina, E.A.; Kochubey, V.I.; Tuchin, V.V. Optical properties of human skin, subcutaneous and mucous tissues in the wavelength range from 400 to 2000 nm. *J. Phys. D Appl. Phys.* **2005**, *38*, 2543–2555. [CrossRef]
24. Federal Communications Commission (FCC). *Revision of Part 15 of the Commission's Rules Regarding Ultra-Wideband Transmission Systems, First Report and Order*; Federal Communications Commission: Washington, DC, USA, February 2002; pp. 1–118.